Numerical Modeling of Space Plasma Flows: ASTRONUM-2013
ASP Conference Series, Vol. 488
N. V. Pogorelov, E. Audit, and G. P. Zank, eds.

Dual Time Stepping Method For three-dimensional MHD With Splitting Based Scheme

Xueshang Feng and Huazheng Fu

SIGMA Weather Group, State Key Lab of Space Weather, Center for Space Science and Applied Research, Chinese Academy of Sciences, PO Box 8701, Beijing 100190, China

Abstract. A new numerical scheme of combining an E-CUSP (energy-convective upwind and split pressure) method for the fluid part and the constrained transport (CT) for the magnetic induction part is proposed by following Shen et al. (2012). Ziegler CT (Ziegler 2004) is used for the magnetic induction part. Meanwhile, in order to avoid the occurrence of negative pressure in both reconstructed and updated profiles, a mixed method of positivity preserving method is used. Furthermore, the MHD equations are solved at each physical time step by advancing in pseudo time. As an independently developed three-dimensional MHD code, the present scheme combined with positivity preserving method and dual time technique has demonstrated the accurateness and robustness through numerical experiments of benchmark problems such as the 2D Orszag-Tang vortex problem and the 3D blast wave problem.

1. Introduction

The characteristic of CUSP (convective upwind and split pressure) schemes is that it simultaneously consider the convective upwind characteristics and avoid the complex matrix dissipation such as that of the Roe's flux difference splitting scheme. The CUSP family can be basically categorized into two types: the H-CUSP and E-CUSP (Jameson 1995). The H-CUSP scheme has total enthalpy in the energy equation in the convective vector, so the scheme is not fully consistent with the disturbance propagation that may affects the stability and robust of the H-CUSP scheme. While, the E-CUSP schemes use total energy in the convective terms, which result in splitting the eigenvalues of the Jacobian to convection (velocity) and waves (speed of sound).

The wave-like structure of the MHD is analogous to that of the hyperbolic systems and thus the E-CUSP scheme have been extended by Shen et al. (2012) to the full set of MHD equations, and the constraint transport (CT) method (Balsara and Spicer 1999) acts as the role of keeping the divergence constraint $\nabla \cdot \mathbf{B} = 0$ and a correction step for cell center magnetic field. The E-CUSP for MHD introduced by Shen et al. (2012) has low diffusion and are able to capture the crisp shock waves and exact contact discontinuities. In reality, the MHD equations can be split into a fluid part leading to an extended Euler system with magnetic force as source and a magnetic induction part (Fuchs et al. 2009; Ziegler 2004). In this paper, we use E-CUSP method to solve the fluid part of MHD, and apply the CT method (Ziegler 2004, 2005) to the magnetic induction part to update the cell face magnetic field. In order to maintain the positivity of pressure and density in the reconstructed profile within the zone for problems in-

volving multiple, interacting shock waves in complex flow, a self-adjusting positivity preserving method by Balsara (2012) is used. The method examines the local magnetic speed to detect regions with strong shock. By visiting the neighboring zones that have connectivity with a zone of interest, we are able to identify minimum and maximum values for density and pressure that should bound the reconstructed profile within the zone of interest (Balsara 2012). Then, weighted mean of the reconstructed conserved variable and the conserved variable is used to correct the reconstructed variable. The self-adjusting positivity preserving method is easy and inexpensive to implement and the result shows that this method can efficiently enhance the robustness.

In the three-dimensional simulation, time steps should be dictated by numerical stability, so they are much smaller than required by accuracy considerations, which will increase computer time for conditionally stable time-marching schemes. To improve computational efficiency, schemes which can use larger possible time-step sizes permitted by accuracy considerations should be taken into account. Here, we use the dual time step scheme to update the conserved variables for flow and magnetic field. Dual time step, which do not modify the original transient evolution of the governing equation, adds to the governing equation a pseudo-time derivative. It uses the pseudo-time steady-state solution to approach the physical-time solution. The advantage of dual time step is that it may possibly speed up the computational efficiency and extend the range of plasma β value.

The paper is organized as follows. In Section 2, the hybrid scheme of combining E-CUSP for the fluid part of MHD and the constraint transport method for the magnetic induction part with dual time stepping are described. In Section 3, two benchmark problems of Orszag-Tang vortex and blast wave are shown. Finally, conclusions are made.

2. Numerical method for MHD equations

The ideal MHD equation for inviscid flow can be expressed as:

$$\frac{\partial \rho}{\partial t}+\nabla\cdot(\rho\mathbf{u}) = 0,\ \frac{\partial \rho\mathbf{u}}{\partial t}+\nabla\cdot(\rho\mathbf{uu}+p_t\mathbf{I}-\mathbf{BB}) = 0,\ \frac{\partial \rho e}{\partial t}+\nabla\cdot((\rho e + p_t)\mathbf{u} - \mathbf{B}(\mathbf{B}\cdot\mathbf{u})) = 0 \quad (1)$$

$$\frac{\partial \mathbf{B}}{\partial t} + \nabla\cdot(\mathbf{uB} - \mathbf{Bu}) = 0 \quad (2)$$

where ρ is the flow density, $\mathbf{u} = (u, v, w)$ is the flow velocity, $\mathbf{B}$ is the magnetic field, p is the pressure, ρe is the total energy, and $p_t = \frac{1}{2}\mathbf{B}^2 + p$.

In this paper, following the idea of Fuchs et al. (2009) we split the MHD equations into a fluid part Eqs. (1) and a magnetic induction part Eq. (2), and employ the E-CUSP for the fluid part and CT scheme for the magnetic induction part in order to get a scheme for full MHD equations (Fuchs et al. 2009). The fluid part Eqs. (1) is approximated by E-CUSP (Shen et al. 2012), and the magnetic part (2) is solved using the divergence-free constraint preserving schme of the constrained transport method (Ziegler 2004, 2005). These two sets of schemes can be combined either component by component, or by using an operator splitting procedure to produce a full scheme for the MHD equations. This is, piecing them together, the resulting update full scheme for MHD equations reads

$$\bar{\mathbf{B}}_f^{n+1} = W^{\mathrm{CT}}\left(\mathbf{U}_{...}^n, \bar{\mathbf{B}}_{...}^n, \delta t^n\right),\ \mathbf{U}_{i,j,k}^{n+1} = V^{\mathrm{E-CUSP}}\left(\mathbf{U}_{...}^n, \bar{\mathbf{B}}_{...}^n, \delta t^n\right)$$

where (i, j, k) stands for the cell center $\bar{\mathbf{B}}_f$ represents magnetic field at the face centers $B_{xi\pm\frac{1}{2},j,k}$, $B_{yi,j\pm\frac{1}{2},k}$, and $B_{zi,j,k\pm\frac{1}{2}}$.

For convenience, we can write the semi-discretized form for the fluid part for Eqs. (1) as follows

$$\frac{\partial \mathbf{U}}{\partial t} + \frac{\mathbf{F}_{i+\frac{1}{2},j,k} - \mathbf{F}_{i-\frac{1}{2},j,k}}{\delta x} + \frac{\mathbf{G}_{i,j+\frac{1}{2},k} - \mathbf{G}_{i,j-\frac{1}{2},k}}{\delta y} + \frac{\mathbf{H}_{i,j,k+\frac{1}{2}} - \mathbf{H}_{i,j,k-\frac{1}{2}}}{\delta z} = 0 \tag{3}$$

with each term having its usual meaning. Following the E-CUSP scheme of Shen et al. (2012) we decompose the flux $\mathbf{F}$ to convective and generalized wave fluxes:

$$\mathbf{F} = \mathbf{f}u + \mathbf{P} + \psi u \tag{4}$$

where

$$\mathbf{f} = [\rho, \rho u, \rho v, \rho w, \rho e]^{\mathrm{T}}\,,\ \psi = [0, 0, 0, 0, p_t]^{\mathrm{T}}$$
$$\mathbf{P} = \left[0, p_t - B_x B_x, -B_y B_x, -B_z B_x, -B_x(uB_x + vB_y + wB_z)\right]^T\,,$$

with the numerical flux at the interface being evaluated in the same way as that given by Shen et al. (2012). Here, in order to achieve second order spatial accuracy, the monotone upstream-centered (MUSCL) reconstruction scheme is used to reconstruct the flow variable. Following Ziegler (2004, 2005), the reconstruction of magnetic field can be achieved by using values at the centers of the cell surfaces.

Shen et al.'s E-CUSP (Shen et al. 2012) uses the WENO reconstruction to compute all the eight equations on zone cell centers by the E-CUSP scheme, then in order to preserve the divergence free condition, they employ Balsara and Spicer CT (Balsara and Spicer 1999) to compute the cell face magnetic field, and finally use the cell face magnetic field to modified the energy.

In our scheme, we split the MHD equations into fluid part and magnetic part, then use different schemes to deal with each part. In fact, the E-CUSP scheme with the MUSCL reconstruction is only used to solve the fluid part on the cell centers, while the magnetic field is obtained with Ziegler CT with van Leer's TVD slope limiter on the cell faces. In Ziegler's scheme, all the reconstruction is based on the staggered magnetic field components without cell-centered magnetic field involved. Thus, there is only one set of magnetic field updated at the face center. The magnetic fields stored on the faces $\mathbf{B}_f$ are only averaged to the zone center value $\mathbf{B}$ when we solve the entropy equation for positivity consideration below.

Positivity of density and pressure may be lost in updating the unknowns at next time step somewhere within a zone or during the reconstruction procedure in obtaining the reconstructed values at the cell interface. In order to avoid the negativeness of density and pressure in the reconstruction and updating procedure, we take the following methods. First, to preserve the positivity for constructed variables, we follow the self-adjusting positivity-preserving method proposed by Balsara (2012). Second, to insure the positivity of the updated variables for each new time level, if the pressure is negative, we turn to solve the entropy equation $\frac{\partial}{\partial t}(\frac{p}{\rho^{\gamma-1}}) + \nabla \cdot (\mathbf{u}\frac{p}{\rho^{\gamma-1}}) = 0$. In our tests, the combination of Balsara's and switches from energy equation to entropy equation is sufficient for the positivity.

2.1. Time integration with dual time stepping

To improve the computational efficiency, we use a backward differentiation in time integration with dual time stepping to advance time marching. The scheme added to the governing equations a pseudo-time derivative emulates the original physical-time derivative. Our dual time stepping formulation for Eqs. (3) reads

$$\frac{\mathbf{U}_{i,j,k}^{n+1,m+1}-\mathbf{U}_{i,j,k}^{n+1,m}}{\delta\tau}+\frac{3\mathbf{U}_{i,j,k}^{n+1,m+1}-4\mathbf{U}_{i,j,k}^{n}+\mathbf{U}_{i,j,k}^{n-1}}{2\delta t}=$$
$$-\frac{\mathbf{F}_{i+\frac{1}{2},j,k}^{n+1,m+1}-\mathbf{F}_{i-\frac{1}{2},j,k}^{n+1,m+1}}{\delta x}-\frac{\mathbf{G}_{i,j+\frac{1}{2},k}^{n+1,m+1}-\mathbf{G}_{i,j-\frac{1}{2},k}^{n+1,m+1}}{\delta y}-\frac{\mathbf{H}_{i,j,k+\frac{1}{2}}^{n+1,m+1}-\mathbf{H}_{i,j,k-\frac{1}{2}}^{n+1,m+1}}{\delta z}$$

where, n is the physical time level, m is the pseudotime level (the number of subiterations), $\delta\tau$ is the pseudotime step size, and δt is the physical time step size. After the residual terms in the right hand of the above equation are linearized at the $m+1$ pseudotime level with respect to the previous pseudotime level m, we arrive at an unfactored implicit form as below

$$\begin{aligned}
&(\frac{1}{\delta\tau}+\frac{3}{2\delta t})\delta\mathbf{U}_{i,j,k}^{n+1,m+1}+\frac{1}{\delta x}(\mathcal{A}_{i+\frac{1}{2},j,k}^{n+1,m}\delta\mathbf{U}_{i+1,j,k}^{n+1,m}-\mathcal{A}_{i-\frac{1}{2},j,k}^{n+1,m}\delta\mathbf{U}_{i-1,j,k}^{n+1,m+1})\\
&=-\frac{3\mathbf{U}_{i,j,k}^{n+1,m}-4\mathbf{U}_{i,j,k}^{n}+\mathbf{U}_{i,j,k}^{n-1}}{2\delta t}-\frac{\mathbf{F}_{i+\frac{1}{2},j,k}^{n+1,m}-\mathbf{F}_{i-\frac{1}{2},j,k}^{n+1,m}}{\delta x}\\
&-\frac{\mathbf{G}_{i,j+\frac{1}{2},k}^{n+1,m}-\mathbf{G}_{i,j-\frac{1}{2},k}^{n+1,m}}{\delta y}-\frac{\mathbf{H}_{i,j,k+\frac{1}{2}}^{n+1,m}-\mathbf{H}_{i,j,k-\frac{1}{2}}^{n+1,m}}{\delta z}-\frac{1}{\delta y}(\mathcal{B}_{i,j+\frac{1}{2},k}^{n+1,m}\delta\mathbf{U}_{i,j+1,k}^{n+1,m}\\
&-\mathcal{B}_{i,j-\frac{1}{2},k}^{n+1,m}\delta\mathbf{U}_{i,j-1,k}^{n+1,m+1})-\frac{1}{\delta z}(C_{i,j,k+\frac{1}{2}}^{n+1,m}\delta\mathbf{U}_{i,j,k+1}^{n+1,m}-C_{i,j,k-\frac{1}{2}}^{n+1,m}\delta\mathbf{U}_{i,j,k-1}^{n+1,m+1})
\end{aligned}\tag{5}$$

with $\mathcal{A}_{i+\frac{1}{2},j,k}^{n+1,m}=\frac{1}{2}\left(\left(\frac{\partial\mathbf{F}}{\partial\mathbf{U}}\right)_{i,j,k}^{n+1,m}+\left(\frac{\partial\mathbf{F}}{\partial\mathbf{U}}\right)_{i+1,j,k}^{n+1,m}\right)$ and the matrices $\mathcal{B}$ and C given like $\mathcal{A}$. Similarly, the above dual time procedure applies to the CT scheme for the magnetic induction part. In each pseudo-time step, the above equation is solved by employing Gauss-Seidel line iteration.

These equations are marched in pseudo time until the derivation of $\mathbf{U}_{i,j,k}$ with respect to τ converges to zero. In simulation, the equations are iterated in pseudo time so that $\mathbf{U}^{n+1,m+1}$ approaches the physical $\mathbf{U}^{n+1}$ as $\left|\mathbf{U}_{i,j,k}^{n+1,m+1}-\mathbf{U}_{i,j,k}^{n+1,m}\right|/\delta\tau$ converges to zero. In the dual time stepping procedure, a physical-time accurate solution is generated upon convergence towards pseudo-time steady-state per physical-time step. In practice, it is not necessary for the the derivation of $\mathbf{U}_{i,j,k}$ with respect to τ to approach zero. As pointed out by Zhao et al. (2008), the convergence criterion can be prescribed by requiring that the residual error $\max(\frac{\delta\rho}{\delta\tau})$ decreases three magnitude. Here, we obtain the conserved variables at $n+1$ time level by choosing $\left|\mathbf{U}_{i,j,k}^{n+1,m+1}-\mathbf{U}_{i,j,k}^{n+1,m}\right|/\delta\tau<1\times10^{-3}$ as the convergence criterion. At the same time, in order to avoid the computation into infinite loop, the maximum iteration steps may be limited. The value of pseudo-time $\delta\tau=\min(\frac{2}{3}\delta t,\mathrm{CFL_{us}}\times V_{i,j,k}/(\lambda_x+\lambda_y+\lambda_z))$ (Jameson 1991) ($\mathrm{CFL_{us}}$ is the usual stability CFL number, and $V_{i,j,k}$ represents the cell volume with λ_x, λ_y, and λ_z the maximum eigenvalues of x, y, z directions respectively.) is suggested such that the matrix involved

in the solver is diagonally dominant and the Gauss-Seidel line iteration can converge. Here, we choose $\delta\tau = dt$, where dt is the physical time restricted only by the stability condition before being enlarged according to Jameson (1991).

Since backward differentiation in time integration involves three time steps, namely $n-1, n$ and $n+1$, a startup procedure is required. Hence, for the first iteration, the explicit second-order Runge–Kutta time stepping that involves two time steps, n and $n+1$, is used to integrate Eq. (2) and Eqs. (3) with the same reconstruction procedure given above.

3. Numerical examples

3.1. 2D: Orszag–Tang vortex

Because the Orszag–Tang vortex problem has interactions of multiple shock waves generated as the vortex evolves, it is considered as one of the standard tests to validate a MHD numerical method. The Orszag–Tang vortex problem is defined on a square domain $[0, 2\pi] \times [0, 2\pi]$ with initial conditions: $\rho = \gamma^2, p = \gamma, u = -\sin y, v = \sin x, B_x = -\sin y, B_y = \sin 2x$, where $\gamma = 5/3$. Periodic boundary conditions are adopted in both coordinate directions. Numerical results are calculated on a N^2 grid with $N = 200, 400$ zones. Figure 1 displays the pressure and B_x contours with a uniform mesh of 200×200 and 400×400 grid points for different CFL conditions.

From Fig. 1, it is evident that at $t = 3$, a fast shock front is formed in the region of $1.25\pi < x < 1.5\pi$ and $0 < y < 0.75\pi$, a slow shock front is formed in the region of $0.5\pi < x < \pi$ and $0.5\pi < y < 0.75\pi$. Our results are quite in agreement with those of Shen et al. (2012), Feng et al. (2006), and Zhou and Feng (2012), although different grids are used.

We investigate the influence of different CFL conditions on the pressure distributions along $y = 1.0$ with the different mesh grids: 200×200 for CFL numbers $0.3, 3.0, 6.0, 9.0$ and 400×400 for CFL numbers $0.3, 6.0, 9.0, 18.0, 24.0, 30.0$. From the numerical results of these tests, we can find the dual time stepping scheme will affect the local maximum and minimum values of the pressure slightly without changing the general structure of the problem. As for their corresponding plots like Fig. 1, we can not discover any difference of the pressure and B_x with these different CFLs. But overall, the scheme works well.

From our experiments, it is found that the convergence criterion for the inner iteration loop is significant in simulating unsteady MHD flows. In the inner iteration, using a given convergence criterion is suggested; if using a maximum iteration step, to ensure the time accuracy and at the same time improve the computational efficiency, we suggest that the maximum iterations are limited in different areas. Near large gradient regions, increasing the inner maximum iteration and refining grid can better enhance the resolution of such variations.

3.2. 3D: blast wave problem

A blast wave problem is a good test of the robustness of a code in modeling 3D shocks and rarefaction. The problem is defined on the 3D Cartesian domain $[-0.5, 0.5]^3$ with initial conditions (Balsara 2012): $B_x = B_y = B_z = 50/\sqrt{3}, \mathbf{u} = \mathbf{0}$, where $\gamma = 1.4$ with unit density. The pressure is set to a value of 1000 inside a central region with a radius of 0.1 and outside the region the pressure is 1.0. In this case, the plasma β is 8×10^{-4}

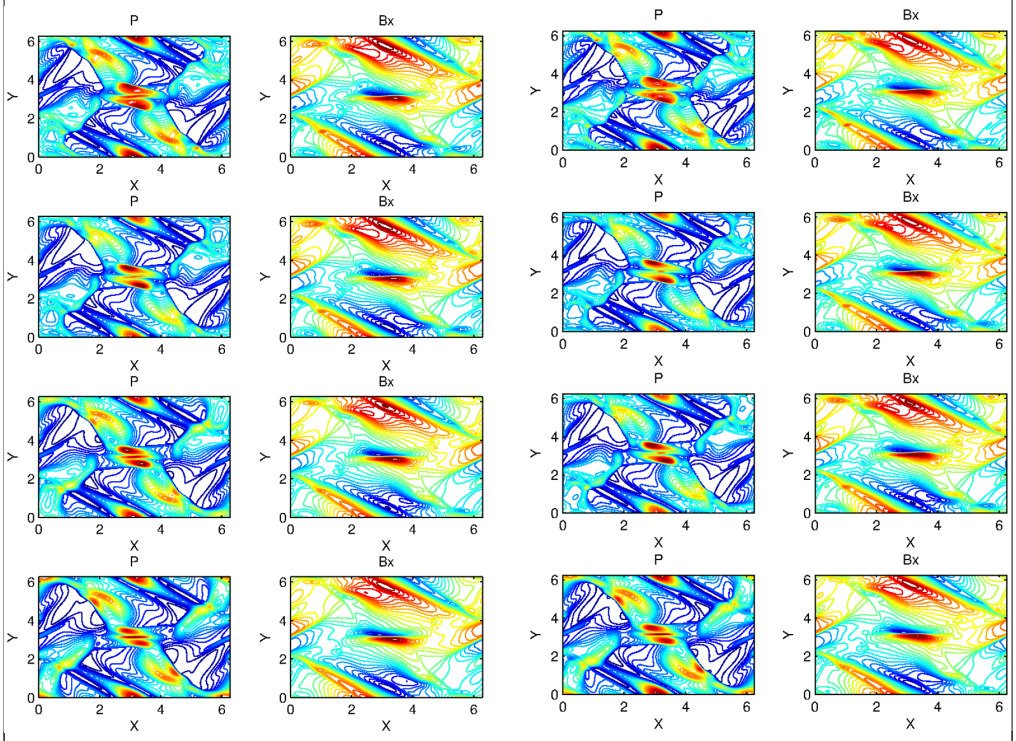

Figure 1. Pressure contour and B_x contours of Orszag–Tang MHD problem with different CFL values with grid meshes 200×200 (*left two columns*) and 400×400 (*right two columns*) at $t = 3.0$. In the left two columns, the CFL number of the first row is 0.3, the second row 3.0, the third row 6.0, the fourth row 9.0. In the right two columns, the CFL number of the first row is 0.3, the second row 6.0, the third row 9.0, the fourth row 18.0.

initially. In order to see the capability of modeling low plasma β, we have another run for $B_x = B_y = B_z = 100/\sqrt{3}$ while keeping the other parameters unchanged, and the plasma β is 2×10^{-5} initially. The blast wave problem becomes stringiest when the plasma β becomes smaller, which can indeed be reached in the solar corona as well as in the magnetosphere of stars and planets. The problem is run up to 0.012. Figure 2 shows the $\log_{10}$ color plot of the density and pressure for the mid-plane in the z-direction with $100 \times 100 \times 100$ grids for $\beta = 8 \times 10^{-4}$ case (top panel) and $\beta = 2 \times 10^{-5}$ case (bottom panel).

In this problem, an almost spherical fast magnetosonic shock propagates through this low-β ambient plasma. From Fig. 2, we can see that there are regions where the strong shock propagates obliquely to the mesh. Our results are quite similar to those of Balsara (2012).

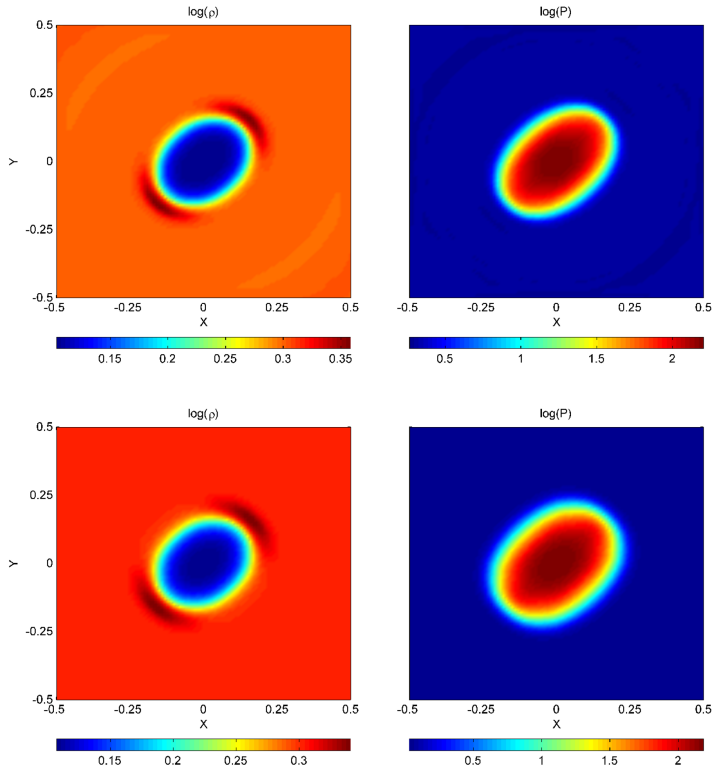

Figure 2. Pressure and B_x contours of blast wave problem from the dual time scheme with grid mesh $100\times100\times100$ for $\beta = 8\times10^{-4}$ (*top panel*) and $\beta = 2\times10^{-5}$ (*bottom panel*) at $t = 0.012$. The CFL number is 4.5.

4. Conclusions

Here is proposed a dual time stepping method with splitting scheme of combing E-CUSP scheme for the fluid part in MHD equations and the constrained transport method for the magnetic induction part. This newly established scheme can avoid the complex eigenstructure of the Jacobian matrices. Backward differentiation in time integration with pseudotime stepping is used to relax the physical time step. Two standard test problems, including the 2D Orszag–Tang vortex problem and the 3D blast wave problem, are solved to validate the accuracy and the robustness of the scheme. The results demonstrate that the scheme can resolve the complex wave characteristics in MHD.

The use of dual time stepping is beneficial in the computation since the use of dual time stepping allows the physical time step not to be limited by the corresponding values in the smallest cell and to be selected based on the numerical accuracy criterion. It is hoped that the present dual time scheme can extend the limitation of the plasma beta in the strong magnetic field region, such as solar coronal magnetic field MHD reconstruction, because of the admittance of enlarged CFL condition. The pseudo time iteration steps required for converngence depend on the CFL number and grid numbers. For example, as for the blast wave problem, when the grid number is $100 \times 100 \times 100$ under enlarged CFL number 30.0, 65 pseudo time iterations are need to meet the 0.001 tolerance, compared to the CFL number 0.3 that will takes 100 iterations. Here, we

only see how much CFL number can be enlarged, without caring much about the computational time. In a pseudo-time, additional acceleration techniques, such as multigrid (Kifonidis and Müller 2012), time-derivation preconditioning (Turkel 1999), should be used without changing the properties of the physical-time in order to explore fast compuational speed. These considerations, combined with the present method's application to the numerical simulation of solar corona (Feng et al. 2011, 2012) will be left for our future work.

Acknowledgments. The work is jointly supported by the National Basic Research Program (973 program) under grant 2012CB825601, the Knowledge Innovation Program of the Chinese Academy of Sciences (KZZD-EW-01-4), the National Natural Science Foundation of China (41031066, 41231068, 41274192, 41174150, and 41374176), and the Specialized Research Fund for State Key Laboratories.

References

Balbás, J., and Tadmor, E., and Wu, C. C., 2004 J. Comput. Phys., 201, 261.
Balsara, D. S., and Spicer, D. S., 1999 J. Comput. Phys., 149, 270.
Balsara, D. S., 2012 J. Comput. Phys., 231, 7504.
Feng, X. S., et al., 2011 Astrophys. J., 734, 50.
Feng, X. S., et al., 2012 Astrophys. J., 758, 62.
Feng, X. S., and Zhou, Y. F., and Hu, Y. Q., 2006 Chin. J. Space Sci., 26, 1.
Fuchs, F. G., and Mishra, S., and Risebro, N., 2009 J. Comput. Phys., 228, 641.
Jameson, A., 1991 AIAA paper, 91-1595.
Jameson, A., 1995 International Journal of Computational Fluid Dynamics, 5, 1.
Kifonidis, K., and Müller, E., 2012 Astron. & Astrophys. , 544, A47.
Shen, Y. Q., and Zha, G. C., and Huerta, M., 2012 J. Comput. Phys., 231, 6233.
Turkel, E., 1999 Annual Review of Fluid Mechanics, 31, 385.
Zhao, R., et al., 2008 Chin. J. Comput. Phys., 25, 5.
Zhou, Y. F., and Feng, X. S., 2012 Chinese Physics Letters, 29, 094703.
Ziegler, U., 2004 J. Comput. Phys., 196, 393.
Ziegler, U., 2005 Comput. Phys. Commun., 170, 153.